# Surface Plasmons Carry the Pancharatnam-Berry Geometric Phase

Salman Daniel, Kimmo Saastamoinen, Toni Saastamoinen, Ismo Vartiainen, Ari T. Friberg, and Taco D. Visser

Phys. Rev. Lett. **119**, 253901 — Published 20 December 2017

DOI: 10.1103/PhysRevLett.119.253901

# Surface plasmon polaritons carry the Pancharatnam–Berry geometric phase

Salman Daniel,[1] Kimmo Saastamoinen,[1] Toni Saastamoinen,[1]
Ismo Vartiainen,[1] Ari T. Friberg,[1] and Taco D. Visser[2,3,4]
[1] *Institute of Photonics, University of Eastern Finland, Joensuu, Finland*
[2] *Department of Physics and Astronomy, Vrije Universiteit, Amsterdam, The Netherlands*
[3] *Department of Physics and Astronomy, University of Rochester, Rochester NY, USA*
[4] *School of Electronics and Information, Northwestern Polytechnical University, Xi'an, China*
(Dated: November 17, 2017)

Surface plasmon polaritons (SPPs) are electromagnetic surface waves that travel along the boundary of a metal and a dielectric medium. They can be generated when freely propagating light is scattered by structural metallic features such as gratings or slits. In plasmonics, SPPs are manipulated, amplified, or routed before being converted back into light by a second scattering event. In this process the light acquires a dynamic phase, and perhaps an additional geometric phase associated with polarization changes. We examine the possibility that SPPs mediate the Pancharatnam–Berry phase, which follows from a closed path of successive in-phase polarization-state transformations on the Poincaré sphere, and demonstrate that this is indeed the case. The geometric phase is shown to survive the light → SPP → light process and, moreover, its magnitude agrees with Pancharatnam's rule. Our findings are fundamental in nature and highly relevant for photonics applications.

PACS numbers: 73.20.Mf, 03.65.Vf, 42.25.Ja

*Introduction.* When a physical system is transported around a closed circuit, it will acquire a phase. This phase is the sum of two parts, a dynamic phase and a geometric phase. The former depends on the time it takes to travel around the circuit, whereas the latter depends on the shape of the path that is taken. Such a geometric phase can occur in a wide range of circumstances [1]. It manifests itself in classical systems, such as Foucault's pendulum [2], but also in quantum systems where it gives rise to the Aharonov–Bohm effect [3]. In both these examples the circuit is a path in ordinary space. However, as pointed out by Berry [4], a quantum system can also acquire a geometric phase when its Hamiltonian is adiabatically moved along a circuit in parameter space. In optics, another geometric phase, also associated with an excursion in parameter space, was identified by Pancharatnam [5]. The state of polarization of a light beam can be represented by a point on the Poincaré sphere [6]. When, with the help of optical elements such as polarizers and wave plates, this polarization state is changed in a cyclical manner, the beam traces out a closed contour on the sphere. Provided the successive states are in phase (Pancharatnam's connection [7]), the associated geometric phase, or Pancharatnam–Berry phase, as it is called, is equal to half the solid angle of the contour subtended at the origin of the Poincaré sphere [8–10]. This result is known as Pancharatnam's rule.

Surface plasmon polaritons (SPPs) are electromagnetic surface waves that propagate along the interface of a metal and a dielectric. In the burgeoning field of plasmonics [11–13] the conversion of light into SPPs and back again is studied. The many promising applications of plasmonics [14] range from ultrafast computer chips and novel biosensors to cloaking devices. In all these examples interference plays a crucial role. It is therefore relevant to explore the phase behavior of SPPs. It is known that the phases of SPP waves (not to be confused with non-propagating, localized surface plasmons [15, 16]) can be controlled through the excitation process, e.g., by illuminating circular gratings [17], concentric circular nanoslits [18], or metasurfaces consisting of arrays of nanorods [19] or nanoslits [20, 21] by light in specific states of polarization. In contrast to these studies, we consider not a single scattering event, but a sequence of in-phase polarization changes (as required by Pancharatnam), which constitute a closed loop on the Poincaré sphere. Further, part of this loop is traversed by SPPs. A question which, to the best of our knowledge, has not been addressed yet, is whether SPPs can carry the topological Pancharatnam–Berry geometric phase, which is a consequence of the curvature of polarization space. And does the Pancharatnam–Berry phase survive the conversion of a light beam into SPPs and back again? These issues are clearly of importance both from a foundational point of view and with an eye to applications. The usual description of polarization changes in terms of Jones algebra [22] cannot shed light on these topics since this formalism simply does not include SPPs. Here we report an experiment which demonstrates conclusively that SPPs can, indeed, mediate the Pancharatnam–Berry geometric phase. Moreover, it is found that this phase remains in existence in the light → SPP → light conversion process, and its magnitude obeys Pancharatnam's rule.

*Theoretical principle.* The conceptual scheme of this work is sketched in Fig. 1. The cyclical polarization change of a monochromatic beam is represented by the closed circuit ABCDEA on the Poincaré sphere. The initial state A, with linear polarization, lies on the equator. The beam then becomes right circularly polarized, state B on the north pole, after passing through a quarter-wave

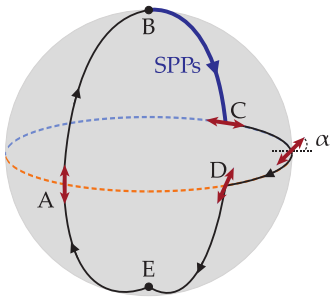


FIG. 1. The closed path ABCDEA on the Poincaré sphere corresponds to successive polarization states. The geodesic arc BC represents the change in polarization that occurs at the conversion of the field into surface plasmons and back again. The angle $\alpha$ specifies the orientation of the linear polarizer acting on the light generated by the plasmons.

plate. It is this light that is used to generate SPPs, which are subsequently converted back into a freely propagating field. This field is in state C on the equator, with a linear polarization that is perpendicular to the initial state A. The light then passes through a linear polarizer with a variable angle of transmission, $\alpha$. This moves the light to another state D, also on the equator. Next, a suitably oriented quarter-wave plate produces left circularly polarized light, indicated by state E on the south pole. A final linear polarizer is used to complete the circuit by bringing the polarization back to state A. In traversing this closed path on the Poincaré sphere the light acquires a Pancharatnam–Berry geometric phase.

Let us denote the solid angle subtended by the circuit at the sphere's origin by $\mathrm{d}\Omega$. As seen from Fig. 1, the two paths ABCA and ADEA together make up the total circuit. We can thus write

$$\mathrm{d}\Omega = \mathrm{d}\Omega_{\mathrm{ABCA}} + \mathrm{d}\Omega_{\mathrm{ADEA}}. \qquad (1)$$

The first solid angle $\mathrm{d}\Omega_{\mathrm{ABCA}} = \pi$, because it corresponds to one fourth of the sphere's surface. The second solid angle, $\mathrm{d}\Omega_{\mathrm{ADEA}}$, depends on the position of state D, i.e., on the transmission angle $\alpha$ of the linear polarizer that is used to produce this state. This angle is taken to be zero when the polarizer completely transmits state C. It is then easily seen that $\mathrm{d}\Omega_{\mathrm{ADEA}} = \pi - 2\alpha$. We now assume, as will be justified later by our experimental results, that Pancharatnam's theorem is also valid when part of the polarization circuit, in this case the geodesic arc BC, is due to a light → SPP → light process. In that case the geometric phase accompanying the circuit, $\delta$, satisfies the relation

$$\delta = \mathrm{d}\Omega/2 = \pi - \alpha. \qquad (2)$$

It follows from this expression that we can control the geometric phase by varying the transmission angle $\alpha$, i.e., by rotating the linear polarizer that changes state C into state D.

*Experiment.* We use a Mach–Zehnder interferometer (see Fig. 2) with a He-Ne laser ($\lambda = 632.8$ nm), whose polarization is set to perpendicular to the optical table (state A). This ensures that the polarization is not changed by beam splitters or mirrors. After beam cleaning and collimation the light is divided into two arms by a 50:50 non-polarizing beam splitter BS1. The field in the lower arm undergoes a series of polarization changes. First it is rendered right circularly polarized, state B, by quarter-wave plate Q1. The beam is then focused normally onto a grating by lens L2 (focal length $f = 11$ mm). This generates SPPs that travel along the sample towards a nanoslit, a distance of 25 $\mu$m from the grating. Here, the plasmons are converted back into a freely propagating field with linear polarization, state C (perpendicular to state A). The emerging field is collected and collimated by a microscope objective OB behind the slit. Next, the beam passes through a rotatable linear polarizer P1 with transmission angle $\alpha$, producing state D on the equator. Quarter-wave plate Q2, joined with P1 such that the ensuing field is always left circularly polarized, generates state E on the south pole. Finally, linear polarizer P2 produces state A, thus completing the circuit. It is crucial that there are no mirrors between Q2 and P2 that might influence the state of polarization. Mirror M3 directs the field onto a 50:50 non-polarizing beam splitter BS2, combining it with the upper arm light. We will demonstrate that this polarization circuit leads to an SPP-mediated Pancharatnam–Berry phase.

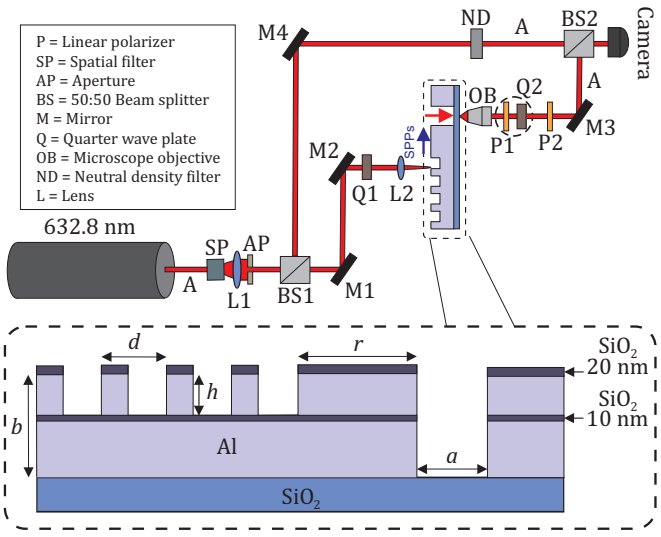


FIG. 2. Schematic of the experimental setup. The components P1 and Q2 are mechanically joined. In the lower part the sample parameters are shown: aluminum layer thickness $b = 400$ nm, grating period $d = 628$ nm, groove height $h = 50$ nm, slit width $a = 200$ nm, and the distance between the grating and the slit $r = 25$ $\mu$m. Thin layers of $SiO_2$ with thicknesses of 20 nm and 10 nm are deposited during fabrication on the top of the sample and inside the grooves.

The field in the upper arm remains in state A, passes through a neutral density filter ND, and is at BS2 combined with the field from the lower arm, creating an interference pattern that is recorded with a CMOS camera. The path length difference is kept within the coherence length of the laser (about 10–30 cm). This, together with the neutral density filter, ensures the production of interference fringes of high visibility. Varying the transmission angle $\alpha$ (by jointly rotating P1 and Q2) changes the solid angle of the circuit on the Poincaré sphere, and thereby alters the geometric phase of the light in the lower arm. This amounts to a changing phase difference between the light in the two arms, leading to a transverse shift of the interference pattern. We measure this shift as a function of the transmission angle $\alpha$.

*Control tests.* The grating is designed by the Fourier modal method [23] to maximize SPP generation. The fabrication of the sample (see inset in Fig. 2), as well as controls which make sure that the light emanating from the slit in Fig. 2 indeed is due to SPPs [24], are described in the *Supplemental Material* [25]. All components are aligned by checking their back reflection of the incoming beam to ensure that the beam passes through the center and that they are free from tilt. To verify this, we use two parallel glass plates instead of polarizer P1 and quarter-wave plate Q2. Almost no change in the interference pattern is observed when the plates are rotated over angles of 20, 40, 60, and 80 degrees, as shown in Fig. 3, with negative angles giving a similar result. This shows that the dynamic phase remains constant when, instead of the glass plates, the joined P1/Q2 element is rotated. Furthermore, to avoid any vibrations these elements are placed on a motorized stage with tunable movement speed.

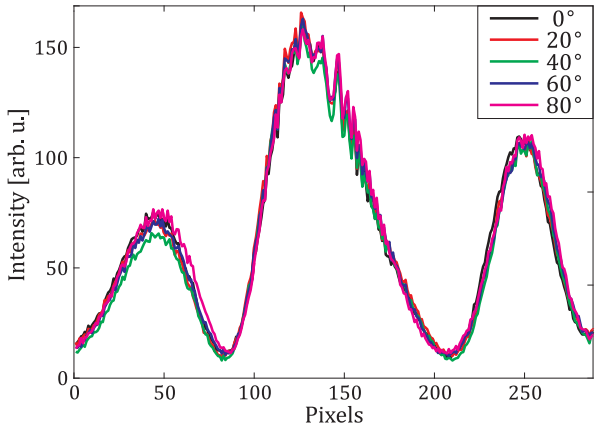


FIG. 3. Interference fringes created by rotating two parallel glass plates over angles of 20, 40, 60, and 80 degrees. No significant change appears in the interference pattern. This demonstrates that the dynamic phase remains constant in our setup.

*Experimental results.* Interference patterns were recorded for different rotation angles $\alpha$ of the combination of P1 and Q2 (Fig. 2). Measurements were performed for $-60° \leq \alpha \leq 60°$ in steps of 20 degrees. For each setting a total of ten repeated measurements were taken to ensure that the phase shifts were not caused by random environmental factors. An example of the raw data is given in Fig. 4(a), where the results of five consecutive measurements for $\alpha = 0°$ and $40°$ are shown. No major variations within the two measurement sets are found, indicating the consistency of the data. These data are then averaged and fitted to a sum of six independent sine curves, as shown in Fig. 4(b). It is seen that the peak to peak distance for a $2\pi$ geometric phase shift is approximately 116 pixels on the horizontal axis. In view of Eq. (2), the phase change introduced by rotating the polarizer over an angle $\alpha$ (from $\alpha = 0$) is equal to $-\alpha$. Therefore, a 1° polarizer rotation should correspond to

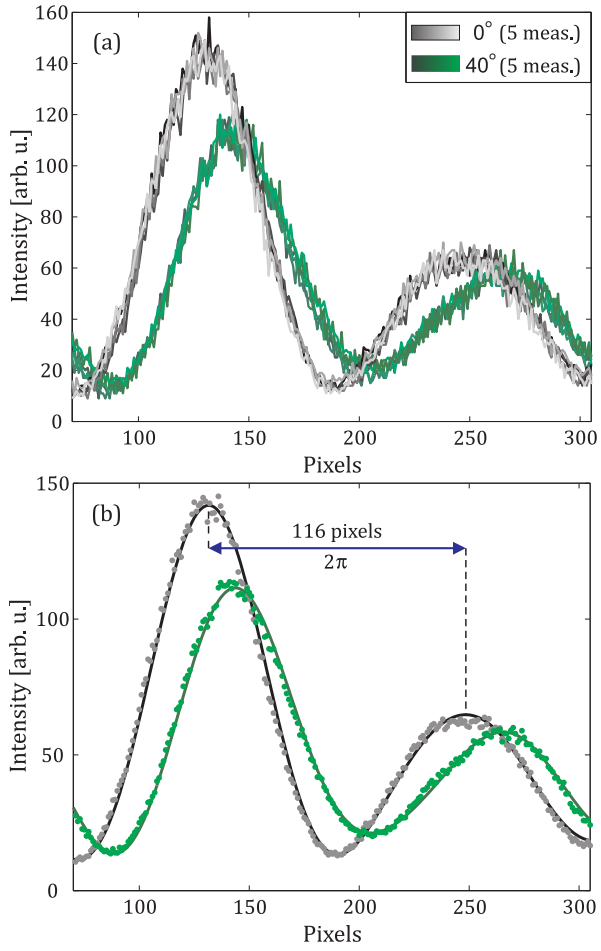


FIG. 4. (a) Five fringe pattern measurements taken for two settings of the transmission angle $\alpha$. Gray shades represent 0°, whereas green shades represent 40°. (b) The average values (dots) of ten successive measurements, and the sine-fitting of these averages (solid curves). The peak to peak distance for the $\alpha = 0°$ curve is 116 pixels.

0.322 pixels. This implies the expected shifts for rotation angles of 20°, 40°, and 60° are 6.4, 12.9, and 19.3 pixels, respectively. Opposite, but equally large, shifts are expected for negative rotation angles.

In Fig. 5 the averaged and fitted data for seven settings of the polarizer are shown. Here the polarizer-wave plate combination is rotated from 0 to 180 degrees, and we show the curves on both sides of the central maximum peak, which is obtained for 0°. Negative angles (−20°, −40°, and −60°) in the figure correspond to 160°, 140°, and 120° of rotation, respectively. The solid curves for positive angles are plotted on the left side of the central peak, whereas the dotted curves for negative angles are plotted on the right side. The vertical dashed line through the maximum of the $\alpha = 0°$ curve helps to establish that the shifts of the peaks are indeed proportional to $\alpha$. It is seen, for example, that the peak shifts for $\alpha = 20°$ and $-20°$ (solid and dotted red curves) with respect to the center peak (solid black curve), are −6 and 8 pixels, respectively. This is in good agreement with the expected value of 6.4 pixels that was mentioned in connection with Fig. 4(b). A similar level of agreement is found for the other polarizer settings.

We took measurements of the interference pattern from a single column of the camera. This way the spatial matching problem of the two beams was minimized. Also, it is seen in Fig. 5 that the intensity of the peaks decreases as we move to higher rotation angles, which is due to the increased blockage of the light by polarizer P1. The intensity of the reference beam is set lower than the maximum throughput intensity at 0° to enhance the visibility of the interference fringes.

The expected and observed fringe shifts, as a function of the polarizer's transmission angle $\alpha$, are plotted in Fig. 6. The seven measured values (open circles) are shown together with their respective error bars. The latter indicate the standard deviation within each set of ten measurements. The straight solid line represents the prediction of Eq. (2), while making use of the fact that, according to Fig. 4(b) and Eq. (2), $d\Omega/d\alpha = 0.322$ pixels/degree. It is clear from Fig. 6 that the observed shift of the interference pattern has a linear dependence on the transmission angle $\alpha$ that is in precise agreement with Pancharatnam's rule, Eq. (2). Furthermore, as was explained above, we ensured that the dynamic phase remained constant during the experiment, and that the light emerging from the slit is due to SPPs. Therefore, the observed shifts are caused by the Pancharatnam–Berry phase that is mediated by SPPs. This implies not only that SPPs carry a topological geometric phase, but also that this phase survives the conversion of a freely propagating field into SPPs, and vice versa. Incidentally, this result is somewhat reminiscent of an earlier report concerning the robustness of quantum entanglement [26].

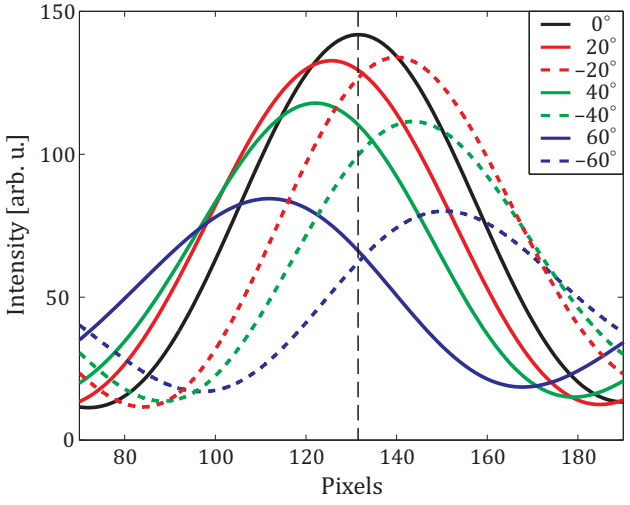


FIG. 5. Shifts in the interference pattern due to a geometric phase carried by SPPs for different angles of rotation of the polarizer. Negative angles (−20, −40, and −60 degrees) in the figure correspond to a 160, 140, and 120 degrees of rotation of the polarizer, respectively.

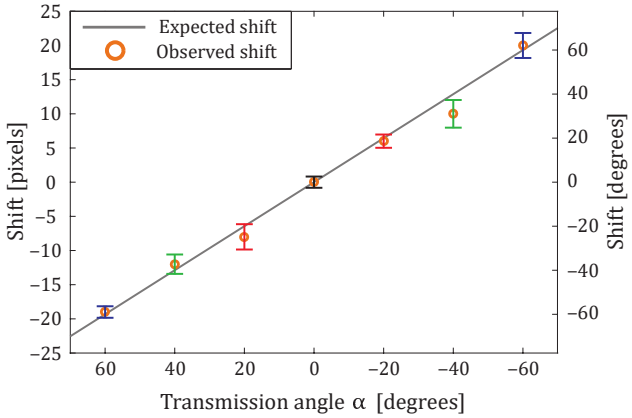


FIG. 6. Expected and observed shifts of the interference fringes as a function of the rotation angle $\alpha$ of the polarizer. The labels on the right show the corresponding phase shift in degrees.

*Conclusions.* We have demonstrated conclusively that surface plasmon polaritons (SPPs), which are highly polarized electromagnetic surface waves propagating on metal-dielectric interfaces, are capable of mediating the Pancharatnam–Berry geometric phase, which is a consequence of the spherical (rather than flat) nature of polarization space. More specifically, we studied a sequence of in-phase polarization changes (as required by Pancharatnam), which together constitute a closed loop on the Poincaré sphere. Part of this loop is traversed by SPPs. The observed geometric phase was shown to be quite robust, as it survives the conversion of light into SPPs and back again. The magnitude of the phase satisfies Pancharatnam's rule. Our finding is of fundamental importance, since phase is an intrinsic, though very

subtle, property of light that governs interference. Our results are also highly relevant for applications in photonics, where conversions between light and SPPs frequently take place and where the geometric phase enables a new generation of versatile optical elements.

*Acknowledgments.* This material is based on work supported by the Air Force Office of Scientific Research (award no. FA9550-16-1-0119), the Academy of Finland (project no. 310511), and the Joensuu University Foundation. K.S. thanks the Magnus Ehrnrooth Foundation for financial support.

[1] A. Shapere and F. Wilczek, eds., *Geometric Phases in Physics* (World Scientific, Singapore, 1989).
[2] M. V. Berry, Phys. Today **43**, 34 (1990).
[3] Y. Aharonov and D. Bohm, Phys. Rev. **115**, 485 (1959).
[4] M. V. Berry, Proc. R. Soc. **A 392**, 45 (1984).
[5] S. Pancharatnam, in *Collected Works of S. Pancharatnam* (Oxford University Press, Oxford, 1975), p. 77.
[6] M. Born and E. Wolf, *Principles of Optics*, 7th ed. (Cambridge University Press, Cambridge, 1999).
[7] M. V. Berry, Curr. Sci. **67**, 220 (1994).
[8] T. H. Chyba, L. J. Wang, L. Mandel, and R. Simon, Opt. Lett. **13**, 562 (1988).
[9] P. Hariharan, in *Progress in Optics*, vol. 48, ed. E. Wolf (Elsevier, Amsterdam, 2005), p. 149.
[10] T. van Dijk, H. F. Schouten, W. Ubachs, and T. D. Visser, Opt. Express **18**, 10796 (2010).
[11] H. Raether, *Surface Plasmons on Smooth and Rough Surfaces and on Gratings* (Springer, Berlin, 1988).
[12] S. A. Maier, *Plasmonics: Fundamentals and Applications* (Springer, Berlin, 2007).
[13] A. A. Maradudin, J. R. Sambles, and W. L. Barnes, eds., *Modern Plasmonics* (Elsevier, Amsterdam, 2014).
[14] H. A. Atwater, Sci. Am. **296**, 56 (2007).
[15] X. Ding, F. Monticone, K. Zhang, L. Zhang, D. Gao, S. N. Burokur, A. de Lustrac, Q. Wu, C.-W. Qiu, and A. Alù, Adv. Mater. **27**, 1195 (2015).
[16] F. Qin, L. Ding, L. Zhang, F. Monticone, C. C. Chum, J. Deng, S. Mei, Y. Li, J. Teng, M. Hong, S. Zhang, A. Alù, and C.-W. Qiu, Sci. Adv. **2**, e1501168 (2016).
[17] K. Y. Bliokh, Y. Gorodetski, V. Kleiner, and E. Hasman, Phys. Rev. Lett. **101**, 030404 (2008).
[18] Y. Guo, M. Pu, Z. Zhao, Y. Wang, J. Jin, P. Gao, X. Li, X. Ma, and X. Luo, ACS Photon. **3**, 2022 (2016).
[19] H. Mühlenbernd, P. Georgi, N. Pholchai, L. Huang, G. Li, S. Zhang, and T. Zentgraf, ACS Photon. **3**, 124 (2016).
[20] L. Huang, X. Chen, B. Bai, Q. Tan, G. Jin, T. Zentgraf, and S. Zhang, Light Sci. Appl. **2**, e70 (2013).
[21] Q. Tan, Q. Guo, H. Liu, X. Huang, and S. Zhang, Nanoscale **9**, 4944 (2017).
[22] C. Brosseau, *Fundamentals of Polarized Light* (Wiley, New York, 1998).
[23] J. Turunen, in *Micro-optics: Elements, Systems and Applications*, ed. H. P. Herzig (Taylor and Francis, London, 1997), p. 31.
[24] S. Daniel, K. Saastamoinen, T. Saastamoinen, J. Rahomäki, A. T. Friberg, and T. D. Visser, Opt. Express **23**, 22512 (2015).
[25] See Supplemental Material at [URL] for the description of sample fabrication and control experiments of SPP generation.
[26] E. Altewischer, M. P. van Exter, and J. P. Woerdman, Nature **418**, 304 (2002).